The Mechanism of GTP Hydrolysis by Dynamin II: A Transient Kinetic Study†

Derk D. Binns,‡ Michael K. Helms,§,|| Barbara Barylko,‡ Colin T. Davis,⊥ David M. Jameson,§ Joseph P. Albanesi,‡ and John F. Eccleston*,⊥

Department of Pharmacology, University of Texas Southwestern Medical Center, Dallas, Texas 75235-9041, Department of Genetics and Molecular Biology, University of Hawaii, Honolulu, Hawaii 96822, and National Institute for Medical Research, Mill Hill, London NW7 1AA, United Kingdom

Received January 7, 2000; Revised Manuscript Received April 7, 2000

ABSTRACT: Dynamin II is a 98 kDa protein (870 amino acids) required for the late stages of clathrin-mediated endocytosis. The GTPase activity of dynamin is required for its function in the budding stages of receptor-mediated endocytosis and synaptic vesicle recycling. This activity is stimulated when dynamin self-associates on multivalent binding surfaces, such as microtubules and anionic liposomes. We first investigated the oligomeric state of dynamin II by analytical ultracentrifuge sedimentation equilibrium measurements at high ionic strength and found that it was best described by a monomer−tetramer equilibrium. We then studied the intrinsic dynamin GTPase mechanism by using a combination of fluorescence stopped-flow and HPLC methods using the fluorescent analogue of GTP, mant*d*GTP (2′-deoxy-3′-*O*-(*N*-methylanthraniloyl) guanosine-5′-triphosphate), under the same ionic strength conditions. The results are interpreted as showing that mant*d*GTP binds to dynamin in a two-step mechanism. The dissociation constant of mant*d*GTP binding to dynamin, calculated from the ratio of the off-rate to the on-rate (k_{off}/k_{on}), was 0.5 μM. Cleavage of mant*d*GTP then occurs to mant*d*GDP and P_i followed by the rapid release of mant*d*GDP and P_i. No evidence of reversibility of hydrolysis was observed. The cleavage step itself is the rate-limiting step in the mechanism. This mechanism more closely resembles that of the Ras family of proteins involved in cell signaling than the myosin ATPase involved in cellular motility.

Dynamin is a 98 kDa protein required for the late stages of clathrin-mediated endocytosis (for reviews, see refs *1*−*4*); mutant forms of dynamin, defective in GTP binding and hydrolysis, have a strong inhibitory effect on clathrin-mediated endocytosis in fibroblast cells (*5*). Dynamin occurs in three known, highly homologous forms in mammalian cells: a neuro-specific dynamin called dynamin I, a ubiquitously expressed isoform called dynamin II, and an isoform expressed exclusively in the testis, lung, and brain called dynamin III (*6*, *7*). Dynamin has been cloned and sequenced, and four structural domains have been identified. The 300 amino acid N-terminal third of the molecule contains a tripartite GTP-binding domain characteristic of other GTP-binding proteins such as Ras. The region from residues 510−620 contains a pleckstrin homology (PH) domain which is known to be involved in binding to PIP_2, an interaction essential to its activity in vivo (*8*−*10*). The region from residues 600−750 contains two putative coiled-coil domains and has been termed the GTPase effector domain (GED) for its ability to stimulate dynamin GTPase activity (*11*). A proline/arginine-rich domain (PRD) extends over 100 residues from amino acid 750 to the C-terminus (residues 864 in rat dynamin I and 870 in rat dynamin II). The PRD domain has multiple proline-rich motifs implicated in protein−protein interactions; specifically this region binds SH3-containing proteins such as Grb2, amphiphysin, and endophilin (*12*).

Dynamin's GTPase is stimulated by several biomolecules including microtubules (*13*), negatively charged phospholipids (*14*), and growth factor receptor binding protein 2 (Grb2) (*15*, *16*). The interaction of dynamin with these biomolecules promotes self-association of dynamin. Dynamin is also known to self-associate in low ionic strength solution, which leads to positive cooperativity in its GTPase activity (*17*). Although the precise role of dynamin is still unknown, it has been proposed to couple the energy released from GTP hydrolysis to the generation of the mechanical force required for membrane fusion during coated vesicle formation (*18*−*20*). However, it has recently been proposed that dynamin is not a force-generating enzyme, but rather is involved in the recruitment of an acyltransferase, endophilin, that promotes endocytosis by altering membrane curvature (*21*, *22*).

Steady-state kinetic methods have generally been used to determine K_m and V_{max} values for the basal GTPase activity of dynamin as well as the enhanced GTPase activity stimulated by factors such as anionic lipids, microtubules, and Grb2. Preliminary transient kinetic studies of the GTPase of bovine brain dynamin I (*23*) have been carried out to determine the elementary processes in the GTPase reaction

† Supported by the National Institutes of Health (Grant GM555620 to J.P.A.), the American Heart Association (Grant 9950020N to D.M.J.), and the Medical Research Council, U.K. (J.F.E.).

* To whom correspondence should be addressed. Tel.: 44 208 959 3666. FAX: 44 208 906 4419. E-mail: jeccles@nimr.mrc.ac.uk.

‡ University of Texas Southwestern Medical Center.

§ University of Hawaii.

|| Present address: LJL Biosystems Inc., 404 Tasman Dr., Sunnyvale, CA 94089.

⊥ National Institute for Medical Research.

10.1021/bi000033r CCC: $19.00
Published on Web 05/24/2000

and to compare them with the kinetic mechanisms of other nucleoside triphosphatases such as myosin ATPase and small G-protein GTPases. For that study, fluorescent analogues of GTP and GDP, 2′(3′)-*O*-*N*-methylanthraniloyl-GTP and -GDP (mantGTP and mantGDP), were utilized. These analogues exist as a mixture of the 2′-O- and 3′-O-substituted nucleotides which may complicate analysis of the data (*24*).

We have now made a detailed transient kinetic study of the intrinsic GTPase of recombinant rat dynamin II using 2′-deoxy-3′-*O*-*N*-methylanthraniloyl-GTP and -GDP (mant*d*GTP and mant*d*GDP)[1] which exist as single substituted derivatives, thus avoiding the problem of working with mixed isomers. This study will serve as a basis for understanding the mechanism of the activation of the GTPase by factors such as Grb2 and phosphoinositides. We have also characterized dynamin II by analytical ultracentrifugation techniques in order to relate the kinetic measurements with the protein's oligomeric state.

MATERIALS AND METHODS

Dynamin II. Dynamin II was purified according to Lin et al. (*38*), and its concentration was estimated using a theoretical extinction coefficient of 53 490 M^{-1} cm^{-1} at 280 nm by the method of Gill and von Hippel (*25*). All measurements were made in buffer containing 20 mM HEPES, pH 7.4, 300 mM NaCl, 5 mM $MgCl_2$, 1 mM EDTA, 0.2 mM phenylmethylsulfonyl fluoride, and 0.5 mM dithiothreitol. Immediately before use, the dynamin solution was centrifuged for 15 min at 100000*g*, 4 °C, to remove any aggregated protein. The analytical ultracentrifugation data were collected at 4 °C. All kinetic measurements were at 20 °C.

Mant-nucleotides. Mant*d*GTP and mant*d*GDP were synthesized, purified, and characterized as described previously (*24*). Their concentrations were determined from their extinction coefficient at 354 nm of 5700 M^{-1} cm^{-1} (*26*).

Stopped-Flow Measurements. Stopped-flow measurements were made using a Hi-Tech MX61 instrument (Hi-Tech, Salisbury, U.K.) operated in the single push mode. All concentrations quoted are those after mixing and so are half of the syringe concentrations. For mant-fluorescence intensity, excitation was at 280 nm unless otherwise stated and emission was monitored through a Wratten 2E cutoff filter (50% transmission at 430 nm, less than 1% transmission at 420 nm). This took advantage of energy transfer between tryptophan residues in dynamin and the mant-fluorophore on the nucleotide which allowed measurements to be made at higher concentrations of mant-nucleotide than could be made by direct excitation at 366 nm (*23*, *27*). All stopped-flow data were fitted to the appropriate equations using Hi-Tech software.

Hydrolysis of MantdGTP. Hydrolysis of mant*d*GTP to mant*d*GDP was monitored by HPLC. Fifty microliters of the dynamin II/mant*d*GTP reaction mixture was added to 5 μL of 0.25% perchloric acid (pH <2), and then 5 μL of 0.4 M sodium acetate was added to adjust the pH to ~4. After centrifugation to remove denatured protein, the supernatant was loaded onto a Novapak C18 (150 × 3.9 mm) HPLC column (Waters) equilibrated with 100 mM potassium phosphate, pH 6.0, 12.5% acetonitrile and eluted isocratically at 0.75 mL min^{-1} with the same buffer. The eluant was monitored using a Hitachi F1050 fluorescence detector with excitation at 366 nm and emission at 440 nm. The signal was recorded using a Hewlett-Packard 3390A Integrator, and the relative concentrations of mant*d*GTP and mant*d*GDP were calculated.

Equilibrium Analytical Ultracentrifuge Measurements. Equilibrium analytical ultracentrifuge measurements were made with a Beckman XL-I analytical ultracentrifuge using a 4-position An60Ti rotor. Each cell had a 6-channel carbon−epon centerpiece with two quartz windows giving an optical path length of 1.2 cm. Each data set represents the average of 15 scans. Each cell was scanned stepwise (0.002 cm steps) at a wavelength of 280 nm and absorbance monitored relative to buffer. After equilibrium was reached (from 24 to 40 h), overspeed runs at 42 000 rpm were carried out to obtain baseline values of absorbance which were used in subsequent fits. The partial specific volume of dynamin II, 0.730 cm^3 g^{-1} at 4 °C (0.737 cm^3 g^{-1} at 20 °C), was calculated from its amino acid composition, and the calculated monomeric molecular weight of $(His)_6$-tagged dynamin II is 99 053. The solvent density was calculated to be 1.013 g·mL^{-1} at 4 °C. Solutions of between 1.5 and 12 μM dynamin II were centrifuged at 7000 rpm at 4 °C until equilibrium had been reached. All data sets were fitted to the appropriate equation using Beckman Optima XL-A/XL-1 data analysis software, version 4.0, either individually or collectively. Figures were replotted using Sigmaplot.

RESULTS

Sedimentation Equilibrium Measurements. To define the oligomeric state of dynamin II under the ionic strength conditions used for the kinetic studies, sedimentation equilibrium measurements were first made. As described under Materials and Methods, dynamin at a range of concentrations was centrifuged at 7000 rpm until equilibrium was reached. The data at three of these concentrations of dynamin II are shown in each panel of Figure 1 together with the best fit of the data to models of (A) a monomer−tetramer, (B) tetramer alone, and (C) dimer−tetramer. These three models all gave reasonable fits to the data whereas with other models, there was a clear discrepancy between the data and the theoretical line. Figure 1 also shows the residuals between the data at 5 μM dynamin and the fitted line for each of these models. It can be seen that the tetramer alone model shows a systematic deviation of the residuals. However, both the monomer−tetramer and dimer−tetramer models fit the data well. This result is in agreement with the in vivo data of Okamo et al. (*28*) and the in vitro analysis of Muhlberg et al. (*11*) that dynamin exists primarily in an oligomeric state.

Analysis of each data set separately to the monomer−tetramer model gives values for the equilibrium constant for the oligomerization of between 1.38 and 3.36 μM^{-3}. There was no correlation between the loading concentration and the equilibrium constant obtained. Fitting all of the data sets simultaneously to a monomer−tetramer model gave a value for the equilibrium constant of 1.92 μM^{-3} with a lower limit of 1.37 μM^{-3} and an upper limit of 2.76 μM^{-3}. Similar

[1] Abbreviations: mant*d*GTP, 2′-deoxy-3′-*O*-*N*-methylanthraniloyl guanosine 5′-triphosphate; the 5′-diphosphate is similarly abbreviated.

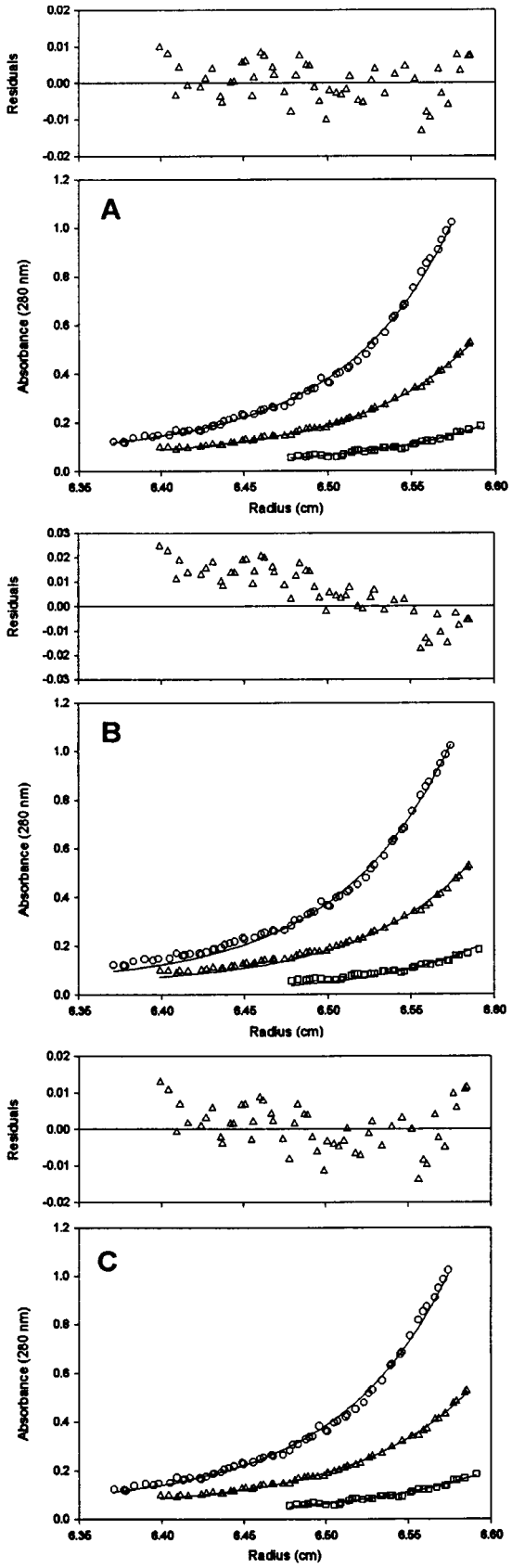

FIGURE 1: Sedimentation equilibrium analytical ultracentrifugation data of dynamin. Solutions of dynamin at initial concentrations of 1.5 μM (□), 5 μM (△), and 10 μM (○) were centrifuged at 7000 rpm until equilibrium was reached. The same data are shown in all three panels with fits to the (A) monomer−tetramer model, (B) tetramer alone model, and (C) dimer−tetramer model. Above these data are the residuals between data and fitted lines for the 5 μM data.

treatment of the data using a dimer−tetramer model gave values for the equilibrium constant from fits to separate data sets between 2.13 and 3.46 μM^{-1} whereas fitting all the data sets simultaneously gave a value for the equilibrium constant of 1.88 μM^{-1} with a lower limit of 1.54 μM^{-1} and an upper limit of 2.35 μM^{-1}.

The variance of the monomer−tetramer fit is slightly better, but not significantly better, than for the dimer−tetramer fit. Thus, with the available data we cannot distinguish between these two models. We previously proposed that dynamin I existed as a monomer−tetramer model under these conditions (*23*). We have reexamined these data and fitted it to both monomer−tetramer and dimer−tetramer models. The dimer−tetramer model did not fit the data well, particularly at the lower concentrations of dynamin I. We therefore suggest that both dynamin I and dynamin II exist as a monomer−tetramer equilibrium.

Using the equilibrium constant for the monomer−tetramer model and calculating the concentrations of monomer and tetramer (based on monomeric concentration) with respect to total dynamin concentration show that equal amounts of monomer and tetramer occur at 1 μM. A similar calculation for the dimer−tetramer model shows that equal amounts of dimer and tetramer also occur at 1 μM. Therefore, whichever model is used does not change the interpretation of the kinetic results.

Binding of MantdGTP and MantdGDP to Dynamin. The binding of mant*d*-nucleotides to dynamin was investigated under pseudo-first-order conditions by monitoring energy transfer between tryptophan in the dynamin and the mant-fluorophore. Figure 2a shows that on mixing 1 μM dynamin with 30 μM mant*d*GTP, there is an increase in fluorescence intensity of 20% which can be well fitted to a single exponential with a rate constant of 75 s^{-1}. The dependence of the observed rate constant of binding of mant*d*GTP to dynamin was investigated over the range of 5−70 μM mant*d*GTP. As the concentration of mant*d*GTP increased, the background fluorescence signal also increased with a reduction in the signal from the binding reaction. Therefore, measurements could not be made above this concentration. The dependence of the observed rate constant of binding of mant*d*GTP to dynamin on mant*d*GTP concentration is shown in Figure 3a. Although this is linear at lower concentrations, there is evidence of hyperbolic behavior at higher concentrations.

There are several possible mechanisms of binding of mant*d*GTP to dynamin that could give rise to this type of behavior. These are described by Bagshaw et al. (*29*) in interpreting their results of the binding of ATP to myosin subfragment 1. The one possibility considered here is that the hyperbolic behavior arises from the binding of mant*d*GTP to dynamin being a two-step process in which there is a rapid equilibrium to form a collision complex, followed by an isomerization of this complex in a process which reports the change of fluorescence intensity:

Scheme 1

$$\text{dynamin} + \text{mant}d\text{GTP} \overset{K_{1a}}{\rightleftharpoons} \text{dynamin}\cdot\text{mant}d\text{GTP} \underset{k_{-1b}}{\overset{k_{1b}}{\rightleftharpoons}}{}^{\Delta F} \text{dynamin}\cdot\text{mant}d\text{GTP}^*$$

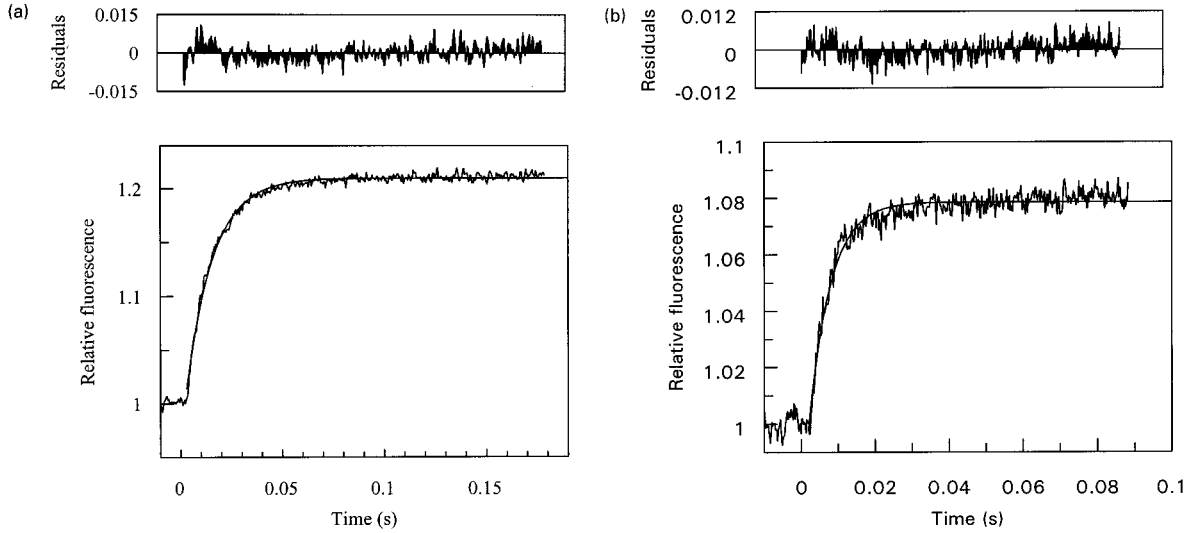

FIGURE 2: Stopped-flow fluorescence record of the binding of mant*d*GTP and mant*d*GDP to dynamin. One syringe contained 1 μM dynamin, and the other syringe contained (a) 30 μM mant*d*GTP and (b) 30 μM mant*d*GDP. The solid lines are best fits to the data to a single exponential giving rate constants of (a) 75 and (b) 171 s^{-1}. The data are the averages of four reactions.

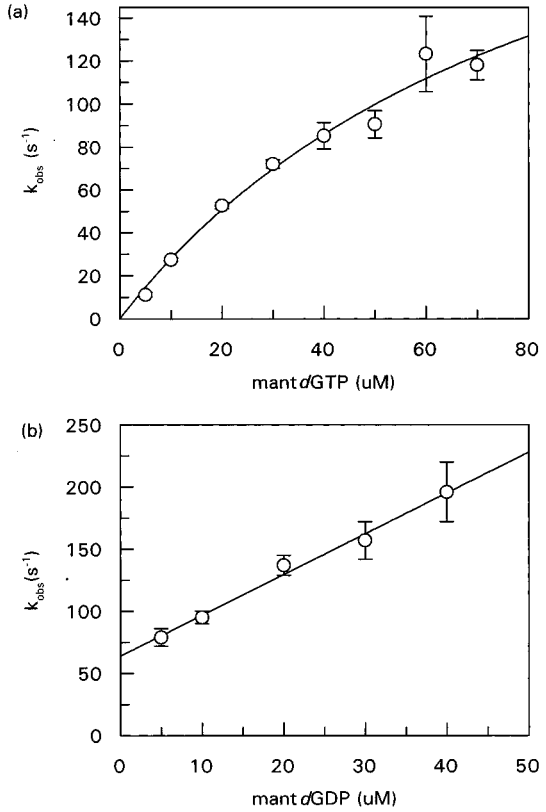

FIGURE 3: Dependence of the observed rate constant of the binding of mant*d*GTP and mant*d*GDP to dynamin on nucleotide concentration. Observed first-order rate constants were obtained from data as shown in Figure 2 and plotted against the concentration of (a) mant*d*GTP and (b) mant*d*GDP. The line in (a) is the best fit of the data to eq 1 with $K_1 = 1.1 \times 10^4$ M^{-1} and $k_2 = 281$ s^{-1}. (b) The line is the best fit to eq 3 with $k_1 = 3.3 \times 10^6$ M^{-1} s^{-1} and $k_{-1} = 64$ s^{-1}.

If this is the case, then the observed rate constant of the process will be given by

$$k_{obs} = k_{1b}/\{1 + 1/(K_{1a}[\text{mantdGTP}])\} + k_{-1b} \quad (1)$$

where K_{1a} is the association equilibrium constant of step 1 and k_{1b} and k_{-1b} are the rate constants for the forward and backward processes of step 2. (This treatment assumes that any subsequent processes are very slow compared to the binding and dissociation processes. This is a valid assumption; see below.)

The solid line in Figure 3a is a fit of the data to this equation giving values of $K_{1a} = 1.1 \times 10^4$ M^{-1} (which is equivalent to a K_d of 91 μM) and $k_{1b} = 280$ s^{-1}. However, because the range of mant*d*GTP concentration is limited to 70 μM, there may be considerable errors in these values. The intercept, as seen in the above equation, gives the value of k_{-1b} but is too close to the origin to define exactly. When $k_{obs} \ll k_{1b}$, then eq 1 reduces to

$$k_{obs} = K_{1a}k_{1b}[\text{mant}d\text{GTP}] \quad (2)$$

Therefore, the slope of the line at low concentration of mant*d*GTP is $K_{1a}k_{1b}$, giving an apparent second-order binding constant of 3.0×10^6 M^{-1} s^{-1}.

Similar binding measurements were made with mant*d*GDP. Again an exponential increase in fluorescence occurred, but this was faster and of smaller amplitude than that observed for mant*d*GTP. For example, at 30 μM mant*d*GDP, the observed rate constant was 171 s^{-1}, and the increase in fluorescence was 8% (Figure 2b). This faster and smaller process limited measurements of mant*d*GDP binding to dynamin to the range of 5−40 μM.

The observed constant of this process was shown to be linearly dependent on mant*d*GDP concentration (Figure 3b). This is the expected behavior of a simple one-step binding process:

$$\text{dynamin} + \text{mant}d\text{GDP} \underset{k_{-1}}{\overset{k_1}{\rightleftharpoons}} \text{dynamin}\cdot\text{mant}d\text{GDP}$$

where the observed rate constant is given by

$$k_{obs} = k_1[\text{mant}d\text{GDP}] + k_{-1} \quad (3)$$

On this basis, the slope of the line in Figure 3b gives k_1 as 3.3×10^6 M^{-1} s^{-1} and the intercept gives k_{-1} as 64 s^{-1}. However, the concentration range at which the reaction could be studied was more limited than that of mant*d*GTP, and it cannot be excluded that mant*d*GDP, like mant*d*GTP, also binds to dynamin by a more complex mechanism.

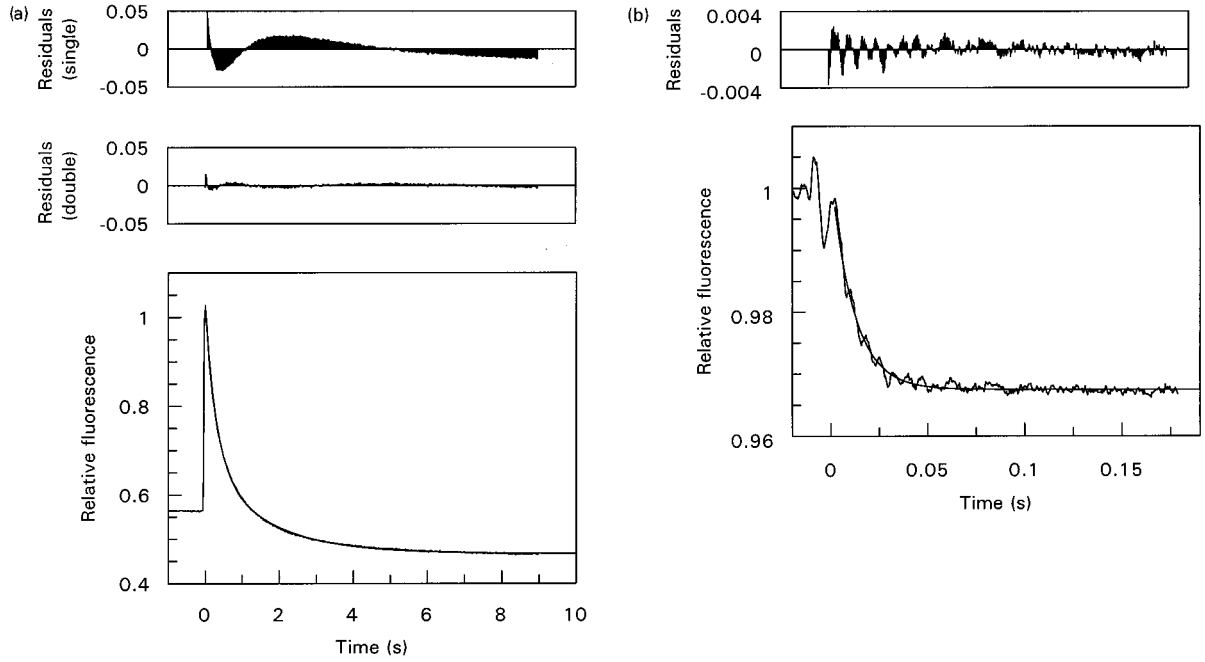

FIGURE 4: Stopped-flow fluorescence record of the displacement of mant*d*GTP and mant*d*GDP from dynamin. (a) One syringe contained 1 μM dynamin, 2 μM mant*d*GTP, and the other syringe contained 100 μM GTP. The upper residuals plot is for a fit to a single exponential with a rate constant of 1.4 s^{-1}, and the lower residuals plot is for a fit to a double exponential with rate constants of 3.3 s^{-1} (amplitude 63%) and 0.64 s^{-1} (amplitude 27%). The data were obtained from a single reaction. (b) One syringe contained 1 μM dynamin, 2 μM mant*d*GDP, and the other contained 5 mM GTP. The line is a fit to a single exponential with a rate constant of 86 s^{-1}. The data represent four reactions averaged.

Displacement of MantdGTP and MantdGDP from Dynamin. To gain more information about the dissociation of mant*d*-nucleotides from dynamin, a solution containing dynamin with mant*d*-nucleotide was rapidly mixed with a large excess of GTP. Figure 4a shows that on mixing a solution of 1 μM dynamin, 2 μM mant*d*GTP with a solution of 100 μM GTP, there was a >50% decrease in fluorescence. This could be fitted to a single exponential with a rate constant of 1.4 s^{-1}, but examination of the residuals between the data points and the fitted line showed a systematic deviation (top residuals plot). The data could be better fitted to a double exponential (lower residuals plot) with rate constants of 3.3 s^{-1} (amplitude 63%) and 0.64 s^{-1} (amplitude 27%) (Figure 4a). The data shown in Figure 4a are a single reaction. Average values from four reactions were rate constants of 3.1 $\pm$ 0.3 s^{-1} (amplitude 0.205 $\pm$ 0.008) and 0.60 $\pm$ 0.05 s^{-1} (amplitude 0.121 $\pm$ 0.010).

To investigate this unexpected biphasic displacement of mant*d*GTP from dynamin, several additional studies were made.

First, the concentration of the GTP used to displace mant*d*GTP from dynamin was increased over the range 100 μM to 5 mM. Even at the latter concentration, the reaction was still biphasic although slightly faster. For example, a single-exponential fit gave a value of 1.6 s^{-1} compared to 1.4 s^{-1} at 100 μM GTP.

Second, the concentration of dynamin was varied with the view that the two processes may represent dissociation of mant*d*GTP from either monomeric or tetrameric species. A solution containing either 0.5 or 5 μM dynamin and 5 μM mant*d*GTP was rapidly mixed with 5 mM GTP. In both cases, a biphasic process occurred with no difference in the rate constants or relative amplitudes of the two processes.

Third, the biphasic nature of the dissociation of mant*d*GTP from dynamin was investigated with the view that one phase may represent dissociation of a hydrolysis product of a dynamin·mant*d*GTP complex. Therefore, a solution of 2 μM dynamin and 1 μM mant*d*GTP was rapidly mixed with a solution of 100 μM GTP within 30 s of adding the mant*d*GTP to the dynamin. The reaction was repeated at increasing time intervals after mixing the mant*d*GTP with the dynamin. All of the reaction profiles were best fitted to a double exponential. There was a slight decrease in the rate constant of the fast phase from time zero to 15 min from 3.41 to 2.96 s^{-1}. Also, the rate constant of the slow phase decreased from 0.66 to 0.50 s^{-1} over this time range. However, the relative amplitudes of the two phases remained constant, 67.5 $\pm$ 2.3% for the fast phase and 33.2 $\pm$ 2.3% for the slow phase. Furthermore, the total amplitude of the fluorescence change together with the amplitudes of the individual phases all decreased exponentially with a rate constant of 0.088 s^{-1} (data not shown). This is comparable with the rate constant of the GTP cleavage step (see below).

The displacement of mant*d*GDP from dynamin was then measured by mixing a solution of 1 μM dynamin and 2 μM mant*d*GDP with a solution of 100 μM GTP. Unlike the case with mant*d*GTP, the data could be fitted to a single exponential with a rate constant of 18.2 $\pm$ 1.3 s^{-1}. However, this value is not in agreement with the value of the dissociation rate constant obtained from the binding data (Figure 3b). The concentration of GTP was increased, and the observed rate constant increased until a limiting value was obtained at 5 mM GTP of 88 $\pm$ 15 s^{-1} (Figure 4b). This value could not be obtained more accurately because, unlike most other stopped-flow measurements reported here, excitation was at 366 nm, because of the large inner filter

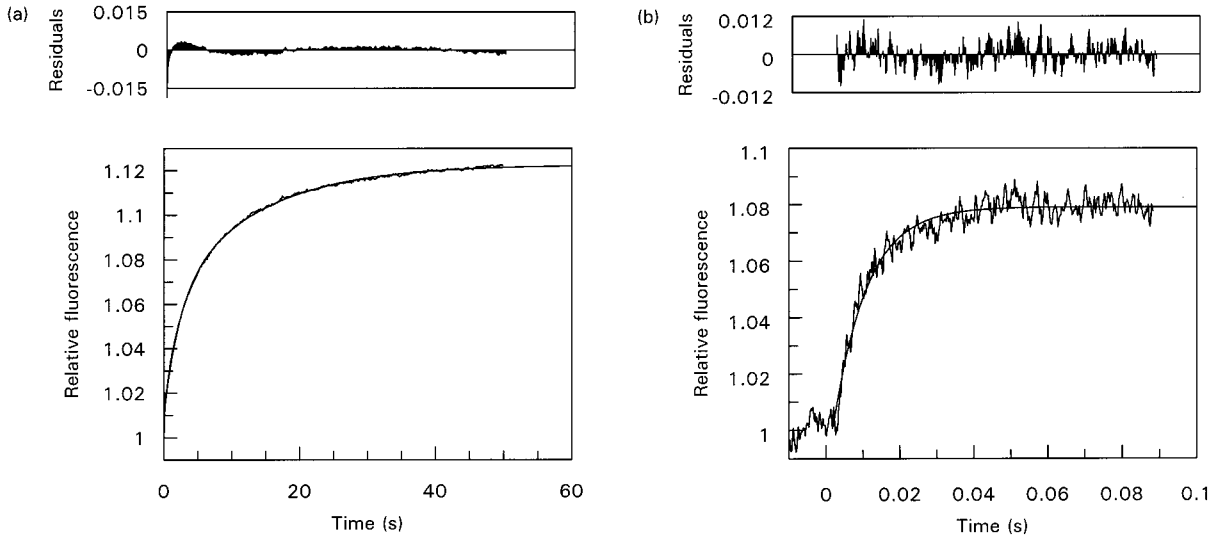

FIGURE 5: Stopped-flow fluorescence record of the displacement of GTP and GDP from dynamin. One syringe contained (a) 1 μM dynamin, 2 μM GTP or (b) 1 μM dynamin, 3 μM GDP, and the other syringe contained 50 μM mant*d*GTP. In (a) the data from a single reaction are shown fitted to a double exponential with rate constants 0.44 s^{-1} (amplitude 44%) and 0.079 s^{-1} (amplitude 56%). In (b) the fit is to a single exponential giving a rate constant of 111 s^{-1}.

effect of 5 mM GTP at 280 nm. This resulted in a reduced signal-to-noise ratio. However, the value of the dissociation rate constant of mant*d*GDP from dynamin by the displacement experiment is now in agreement with that obtained by the binding data. [For a discussion of how displacement experiments can give false values of observed dissociation rate constants, see Gutfreund (*30*).]

Dissociation of GTP and GDP from Dynamin. The dissociation rate constants of GTP and GDP from dynamin were measured by displacing them with mant*d*GTP. On mixing a solution containing 1 μM dynamin and 2 μM GTP with a solution containing 50 μM mant*d*GTP, a 12% increase in fluorescence occurred (Figure 5a). This was not well fitted to a single exponential but could be fitted to a double exponential. The first rate constant was 0.37 $\pm$ 0.01 s^{-1} (amplitude 48%), and the second rate constant was 0.073 $\pm$ 0.003 s^{-1} (amplitude 52%). On repeating the experiment but mixing a solution containing 1 μM dynamin and 3 μM GDP with a solution containing 50 μM mant*d*GTP, a 7% increase in fluorescence occurred which could be fitted to a single exponential with a rate constant of 111 s^{-1} (Figure 5b).

Higher concentrations of mant*d*GTP could not be used to determine if these are the real dissociation rate constants of GTP and GDP from dynamin because of the reduced signal-to-noise ratio resulting from the free mant*d*GTP in solution. However, the values most probably represent a lower limit of these rate constants.

Hydrolysis of MantdGTP by Dynamin. Five micromolar dynamin was mixed with 2.5 μM mant*d*GTP, and the reaction was followed in two ways. First, measurements were made in a stopped-flow instrument, and the fluorescence intensity of the emitted light was measured with excitation at 280 nm. There was first a 3-fold rapid increase in fluorescence intensity followed by a slower decrease in intensity to a value of about 1.3-fold of the intensity before mixing (Figure 6). The fast phase was not well described by a single exponential but would not be expected to since the binding process is not under pseudo-first-order conditions. The slow phase was fitted to a single exponential with a rate constant of 0.0056 s^{-1}.

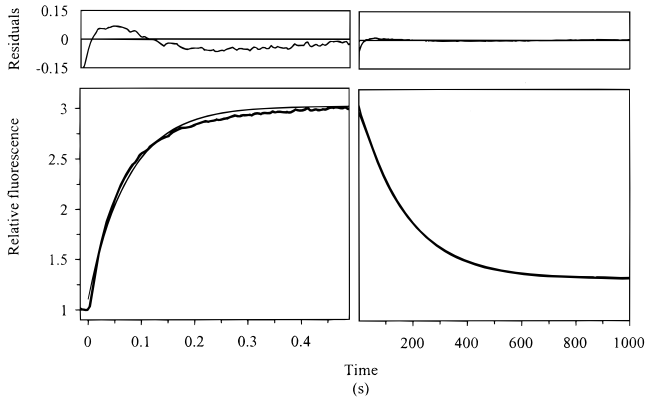

FIGURE 6: Stopped-flow fluorescence record of a single turnover of mant*d*GTP by dynamin. One syringe contained 5 μM dynamin, and the other syringe contained 2.5 μM mant*d*GTP. The time course was followed over 0.5 s (left panel) and 1000 s (right panel). A fit of the slow process to a single exponential gives a rate constant of 0.0056 s^{-1}.

Second, the reaction was repeated, but samples were taken at time intervals, quenched by the addition of perchloric acid, and analyzed for the relative concentrations of mant*d*GTP and mantdGDP by HPLC analysis. Plotting the percentage of mant*d*GTP in the reaction mixture with time showed an exponential decrease of mant*d*GTP with a rate constant of 0.0062 s^{-1} (Figure 7). The fluorescence decrease seen in Figure 6 therefore represents the cleavage step of GTP hydrolysis.

To confirm that there was no rapid formation of mantdGDP by dynamin during the first turnover of mant*d*GTP, a solution containing 5 μM dynamin and 25 μM mant*d*GTP was incubated at 20 °C, and samples were taken to measure the conversion of mant*d*GTP to mant*d*GDP by HPLC. The hydrolysis of mantdGTP by dynamin was linear over the first 300 s of the reaction with no evidence of rapid formation of mant*d*GDP prior to the overall steady-state rate of hydrolysis (data not shown). The steady-state rate of hydrolysis from the linear plot was calculated to be 0.0040 s^{-1}.

Hydrolysis of GTP by Dynamin. To compare the rate of hydrolysis of mant*d*GTP with GTP itself, the formation of

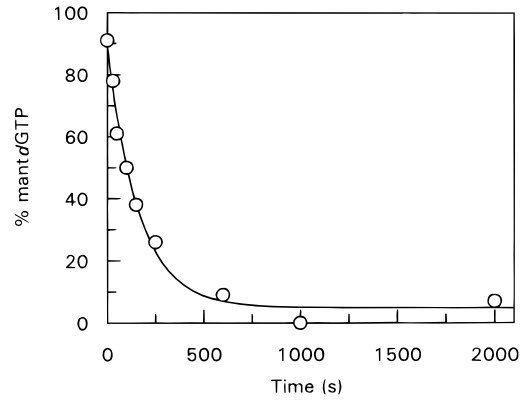

FIGURE 7: Hydrolysis of mant*d*GTP by dynamin. A solution containing 5 μM dynamin and 2.5 μM mant*d*GTP was incubated at 20 °C. Samples were taken at intervals and analyzed for percentages of mant*d*GTP and mant*d*GDP. The line is a fit of the data to a single exponential with a rate constant of 0.0062 s^{-1}.

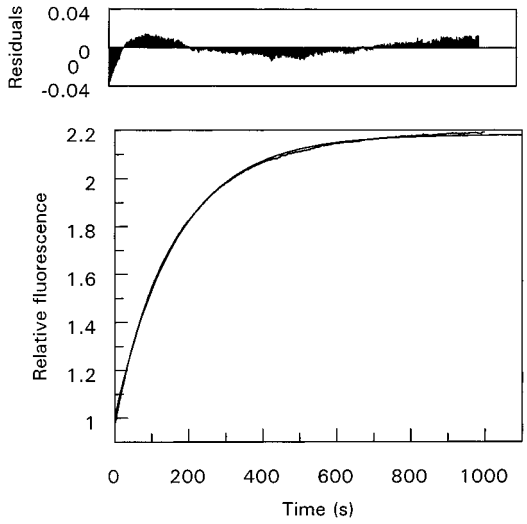

FIGURE 8: Stopped-flow record of the release of P_i during a single turnover of GTP by dynamin. One syringe contained 5 μM dynamin, and the other contained 2.5 μM GTP. Both syringes contained 13 μM coumarin-labeled phosphate binding protein. The solid line is the best fit to a single exponential with a rate constant of 0.0061 s^{-1}.

free P_i during a single turnover of GTP by dynamin was monitored. This was done by performing the reaction in the presence of phosphate binding protein labeled with a coumarin which gives a fluorescence signal on binding of P_i (*31*). A solution of 5 μM dynamin was rapidly mixed with a solution of 2.5 μM GTP in the presence of 13 μM phosphate binding protein (Figure 8). An increase in fluorescence occurred which could be fitted to a single exponential with a rate constant of 0.0061 s^{-1}. Examination of the residuals between the data and the fitted line does show a small systematic deviation, but fitting the data to a double exponential gives rate constants too close to resolve. A control experiment using a higher concentration of GTP showed that the signal from the phosphate binding protein was linear with respect to P_i at the concentration range used.

DISCUSSION

Interaction of Dynamin with MantdGTP and GTP. The binding of mantdGTP to dynamin has been shown not to be a simple one-step process. The data have been interpreted in terms of an initial rapidly reversible process with an equilibrium constant (K_{1a}, Scheme 1) of 1.1 $\times$ 10^4 M^{-1} followed by an isomerization of the dynamin·mant*d*GTP complex with a rate constant of 280 s^{-1}. This results in an apparent second-order binding constant of 3.0 $\times$ 10^6 M^{-1} s^{-1}. However, other mechanisms could explain the data such as an isomerization of the dynamin prior to binding mant*d*GTP or two distinct modes of mant*d*GTP binding to dynamin resulting in an equilibrium mixture of both complexes.

Dissociation of mant*d*GTP from dynamin also shows complex behavior. It occurs as a biphasic process with rate constants of 3.09 $\pm$ 0.30 and 0.60 $\pm$ 0.05 s^{-1} with relative amplitudes of 63% and 27%. We found similar behavior with dynamin 1 and suggested that this may be the result of using mantGTP which consists of an equilibrium mixture of the 2′- and 3′-substituted derivatives (*23*). However, in this study, we have used mant*d*GTP which exists as a single isomer, thus ruling out this as a cause of the biphasic reaction.

A second possibility considered was that the biphasic displacement behavior resulted from displacement of mant*d*GTP from different oligomeric states of dynamin. Using the values of the equilibrium constants obtained from the analytical ultracentrifuge data, the precentage of monomer (or dimer) in solutions of 1 and 10 μM total dynamin concentration can be calculated to be 49% and 11%, respectively. However, on displacing mant*d*GTP from these two different concentrations of dynamin, both gave biphasic processes with similar amplitudes. It should be noted that the ultracentrifugation data were obtained at 4 °C whereas the kinetic experiments were obtained at 20 °C. In our hands, dynamin is not sufficiently stable at 20 °C to make sedimentation equilibrium measurements. To investigate this problem in more detail, the concentration range of dynamin needs to be varied over a larger concentration range. In the present experiments, the upper concentration of dynamin is limited by availability and the lower range by the signal-to-noise ratio of the mant-fluorophore. The development of more sensitive ribose-modified GTP analogues (*24*) will allow measurements at lower concentrations of dynamin to be made.

Whatever the cause of these biphasic displacement data, using the apparent second-order binding constant of 3.0 $\times$ 10^6 M^{-1} s^{-1} and the dissociation rate constants of 3.1 and 0.60 s^{-1}, the values of the K_d of the two forms of dynamin are 1 and 0.2 μM, respectively.

The dissociation of GTP itself was measured by displacement with mantdGTP. Again, this was not well fitted to a single exponential but showed biphasic behavior with rate constants of 0.37 $\pm$ 0.01 and 0.073 $\pm$ 0.003 s^{-1} with relative amplitudes of 48% and 52%. Therefore, both processes have rate constants about 10 times slower than for mant*d*GTP displacement. It is reasonable to assume that the association rate constants of GTP and mant*d*GTP to dynamin are similar. Therefore, GTP binds to dynamin approximately 10 times tighter than mant*d*GTP.

Interaction of Dynamin with MantdGDP and GDP. At first sight, the results on the interaction of mant*d*GDP with dynamin were easier to interpret. The observed first-order rate constants of the binding of mant*d*GDP to dynamin were linearly dependent on mant*d*GDP concentration (Figure 3b). The slope of the line gave a second-order association rate

constant of 3.3×10^6 M^{-1} s^{-1}, and the intercept gave a dissociation rate constant of 64 s^{-1}. Combining these two values gave an equilibrium dissociation constant of 19 μM.

The dissociation of GDP from dynamin was measured by a displacement experiment with mant*d*GTP. This process was also well fitted to a single exponential with a rate constant of 111 s^{-1} (Figure 5b). Again, assuming that the association rate constants of GDP and mant*d*GDP are the same, this implies that if anything, GDP binds more weakly to dynamin than mant*d*GDP. However, the value for GDP dissociation is not accurately determined since a large excess of displacing nucleotide could not be used.

Hydrolysis by Dynamin. In the previous sections, we have addressed the initial interactions of mant*d*GTP and mant*d*GDP with dynamin. To gain an understanding of the hydrolysis mechanism, the interaction of mant*d*GTP with excess dynamin was studied over longer time courses. It was shown that on mixing 5 μM dynamin with 2.5 μM mant*d*GTP that following the binding process, an exponential decrease in fluorescence occurred (Figure 6) with a rate constant of 0.0056 s^{-1}. When this reaction was repeated, but conversion of mant*d*GTP to mant*d*GDP was measured directly, the rate constant for the cleavage step was found to be 0.0062 s^{-1} (Figure 7). Therefore, the slow fluorescence decrease seen in Figure 6 is reporting the cleavage step of the reaction. There was no evidence for any rapid formation of phosphate during the first turnover of mant*d*GTP by dynamin as occurs with the hydrolysis of ATP by myosin subfragment 1 (*32*). The rate constant for GTP hydrolysis determined by monitoring P_i release is 0.0061 s^{-1}, within experimental error identical to that of mant*d*GTP hydrolysis.

These experiments show that following the two-step binding of mant*d*GTP to dynamin, the cleavage of mant*d*GTP to mant*d*GDP is the rate-limiting step in the reaction. This is followed by the release of mantdGDP (at 64 s^{-1}) and P_i although the order of product release cannot be determined.

These results show that the mechanism of hydrolysis of GTP by dynamin shows both similarities and differences with the hydrolysis of GTP by small G-proteins (*33*) and of hydrolysis of ATP by myosin subfragment 1 (*34*). The initial binding step is relatively weak compared to GTP binding to small G-proteins and ATP binding to myosin subfragment 1 although all these processes appear to occur by a two-step mechanism (*29*, *35*). The cleavage step being rate-limiting in the overall hydrolysis reaction and being irreversible is common to the small G-proteins, but differs from the myosin subfragment 1 ATPase where cleavage is fast and reversible. P_i release is fast compared to the cleavage step which is again a feature of the small G-proteins but not myosin subfragment 1. Finally, with dynamin, GDP release is very fast. Here it differs from the small G-proteins in which GDP release, in the absence of exchange factors, is of the same order of magnitude as the cleavage step (*33*).

Activation of dynamin GTPase activity accompanies dynamin self-association, apparently of higher order than tetramerization (*36*). At low ionic strength, this self-association can occur in the absence of other macromolecules. At physiological ionic strength, it is facilitated by anionic scaffolds [PS- or PIP_2-containing liposomes or microtubules (*13*, *37*, *38*)] or cross-linking proteins [Grb2 or anti-dynamin polyclonal antibodies (*39*, *40*)]. Regardless of the mode of GTPase stimulation, our data suggest that it must occur by a mechanism which accelerates the GTP cleavage step. In the case of the small G proteins such as Rac and Rho, this is achieved by a GTPase activating protein (GAP) that promotes hydrolysis by the insertion of a catalytic arginine residue into the active site and by the stabilization of the effector loop (*41*−*43*). In the case of dynamin, this is accomplished by a domain located between amino acids 620 and 746 (in dynamin II) called the GTPase-effector domain (GED), which is believed to act intermolecularly between dynamins (*11*, *44*). At the salt concentrations used in our experiments, dynamin cannot oligomerize into large structures (*45*). Consequently, there is no stimulation of the GTPase activity as a function of dynamin concentration. Therefore, we are characterizing only the basal GTPase activity of dynamin, and the GED interaction is not likely to play a role in the kinetics of GTP hydrolysis by dynamin under the conditions used in this paper.

ACKNOWLEDGMENT

We thank Dr. M. R. Webb for providing the coumarin-labeled phosphate binding protein and for advice on its use.

REFERENCES

1. Hinshaw, J. E. (1999) *Curr. Opin. Struct. Biol. 9*(2), 260−267.
2. McNiven, M. A. (1998) *Cell 94*(2), 151−154.
3. van der Bliek, A. M. (1999a) *Trends Cell Biol. 9*(3), 96−102.
4. van der Bliek, A. M. (1999b) *Trends Cell Biol. 9*(7), 253−254.
5. Damke, H., Baba, T., Warnock, D. E., and Schmidt, S. L. (1994) *J. Cell Biol. 127*(4), 915−934.
6. Cook, T., Mesa, K., and Urrutia, R. (1996) *J. Neurochem. 67*(3), 927−931.
7. Sontag, J. M., Fykse, E. M., Ushkaryov, Y., Liu, J. P., Robinson, P. J., and Sudhof, T. C. (1994) *J. Biol. Chem. 269*(6), 4547−4554.
8. Achiriloaie, M., Barylko, B., and Albanesi, J. P. (1999) *Mol. Cell Biol. 19*(2), 1410−1415.
9. Lee, A., Frank, D. W., Marks, M. S., and Lemmon, M. A. (1999) *Curr. Biol. 9*(5), 261−264.
10. Vallis, Y. Wigge, P., Marks, B., Evans, P. R., and McMahon, H. T. (1999) *Curr. Biol. 9*(5), 257−260.
11. Muhlberg, A. B., Warnock, D. E., and Schmid, S. L. (1997) *EMBO J. 16*(22), 6676−6683.
12. McPherson, P. S. (1999) *Cell Signalling 11*(4), 229−238.
13. Schpetner, H. S., and Vallee, R. B. (1992) *Nature 355*(6362), 733−735.
14. Tuma, P. L., Stachniak, M. C., and Collins, C. A. (1993) *J. Biol. Chem. 268*(23), 17240−17246.
15. Gout, I., Dhand, R., Hiles, I. D., Fry, M. J., Panayotou, G., Das, P., Truong, O., Totty, N. F., Hsuan, J., and Booker, G. W. (1993) *Cell 75*(1), 25−36.
16. Herskovits, J. S., Schpetner, H. S., Burgess, C. C., and Vallee, R. B. (1993b) *Proc. Natl. Acad. Sci. U.S.A. 90*(24), 11468−11472.
17. Tuma, P. L., and Collins, C. A. (1994) *J. Biol. Chem. 269*(49), 30842−30847.
18. Sweitzer, S. M., and Hinshaw, J. E. (1998) *Cell 93*(6), 1021−1029.
19. Takei, K., Haucke, V., Slepnev, V., Farsad, K., Salazar, M., Chen, H., and De Camilli, P. (1998) *Cell 94*(1), 131−141.
20. Kozlov, M. M. (1999) *Biochim. Biophys. Acta 742*(3), 496−508.
21. Ringstad, N., Gad, H., Low, P., Di Paolo, G., Brodin, L., Shupliakov, O., and De Camilli, P. (1999) *Neuron 24*, 143−154.
22. Schmidt, A., Wolde, M., Thiele, C., Fest, W., Kratzin, H., Podtelejnikov, A. V., Witke, W., Huttner, W. B., and Soling, H. D. (1999) *Nature 401*(6749), 133−141.

23. Binns, D. D., Barylko, B., Grichine, N., Atkinson, M. A. L., Helms, M. K., Jameson, D. M., Eccleston, J. F., and Albanesi, J. P. (1999) *J. Protein Chem. 18*, 277−290.
24. Jameson, D. M., and Eccleston, J. F. (1997) *Methods Enzymol. 278*, 363−390.
25. Gill, S. C., and von Hippel, P. H. (1989) *Anal. Biochem. 182*, 319−326.
26. Hiratsuka, T. (1983) *Biochim. Biophys. Acta 742*, 496−508.
27. Woodward, S. K. A., Eccleston, J. F., and Geeves, M. A. (1991) *Biochemistry 30*, 422−430.
28. Okamoto, P. M., Tripet, B., Litowski, J., Hodges, R. S., and Valee, R. B. (1999) *J. Biol. Chem. 274*, 10277−10286.
29. Bagshaw, C. R., Eccleston, J. F., Eckstein, F., Goody, R. S., Gutfreund, H., and Trentham, D. R. (1974) *Biochem. J. 141*, 351−364.
30. Gutfreund, H. (1995) *Kinetics for the Life Sciences*, pp 179−194, Cambridge University Press, Cambridge U.K.
31. Brune, M., Hunter, J., Corrie, J. E. T., and Webb, M. R. (1994) *Biochemistry 33*, 8262−8271.
32. Lymn, R. W., and Taylor, E. W. (1970) *Biochemistry 9*, 2975−2983.
33. Neal, S. E., Eccleston, J. F., Hall, A., and Webb, M. R. (1988) *Proc. Natl. Acad. Sci. U.S.A. 263*, 19718−19722.
34. Geeves, M. A., and Holmes, K. C. (1999) *Annu. Rev. Biochem. 68*, 687−728.
35. John, J., Sohmen, R., Feuerstein, J., Linke, R., Wittinghofer, A., and Goody, R. S. (1990) *Biochemistry 29*, 6058−6065.
36. Warnock, D. E., Baba, T., and Schmid, S. (1997) *Mol. Biol. Cell 8*, 2553−2562.
37. Tuma, P. L., and Collins, C. A. (1995) *J. Biol. Chem. 270*, 26707−26714.
38. Lin, H. C., Barylko, B., Achiriloaie, M., and Albanesi, J. P. (1997) *J. Biol. Chem. 272*, 25999−26004.
39. Barylko, B., Binns, D., Lin, K.-M., Atkinson, M. A. L., Jameson, D. M., Yin, H. L., and Albanesi, J. P. (1998) *J. Biol. Chem. 273*, 3791−3797.
40. Warnock, D. E., Terlecky, L. J., and Schmid, S. L. (1995) *EMBO J. 14*, 1322−1328.
41. Ahmadian, M. R., Stege, P., Scheffzek, K., and Wittinghofer, A. (1997) *Nat. Struct. Biol. 4*, 686−689.
42. Scheffzek, K., Ahmadian, M. R., and Wittinghofer, A. (1998) *Trends Biochem. Sci. 23*, 257−262.
43. Rittinger, K., Walker, P. A., Eccleston, J. F., Smerdon, S. J., and Gamblin, S. J. (1997) *Nature 389*, 758−762.
44. Sever, S., Muhlberg, A. B., and Schmid, S. L. (1999) *Nature 398*, 481−486.
45. Hinshaw, J. E., and Schmid, S. L. (1995) *Nature 374*, 190−192.

BI000033R